Electron-irradiation-induced divacancy in lightly doped silicon

A. O. Evwaraye

General Electric Corporate Research and Development, Schenectady, New York 12301

Edmund Sun

General Electric Company, Semiconductor Products Department, Auburn, New York 13201
(Received 5 April 1976)

Two electron traps—A2 and A3—produced in *n*-type silicon by 1.5-MeV-electron irradiation are characterized by deep level transient spectroscopy. Activation energies of trapped majority carriers and capture cross sections for majority carriers at these levels are reported. From their production rates and annealing behaviors, they have been identified as different charge states of the same defect. Detailed annealing studies show that their annealing kinetics is first order with an activation energy of 1.47 eV. It is suggested that the defect is the divacancy and that dissociation is the likely process for its removal in these devices.

PACS numbers: 61.80.Fe, 61.14.−x, 61.70.Kd

I. INTRODUCTION

There have been many studies of electron-induced defects in silicon. Hall-effect measurements,[1–7] minority-carrier-lifetime studies,[8,9] infrared absorption measurements[10–13] thermally stimulated capacitance (TSCAP),[14,15] and deep level transient spectroscopy (DLTS)[16] have all been used to study the electrical properties of these defects. The use of electron paramagnetic resonance (EPR)[17–21] in determining the microscopic configurations of these defects has been most fruitful.

One of the electron-induced defects unraveled by EPR is the divacancy.[20,21] It is produced either as a multiple displacement defect in the primary radiation damage event or as a combination of two single vacancies. The divacancy is generally believed[20,22] to diffuse within the system until trapped and removed by sinks. An activation energy of 1.25–1.3 eV was determined for this diffusion process from high-temperature stress studies[20,22] and from annealing studies of 1.8- and 3.3-μ bands in the ir spectrum.[22] The binding energy of the divacancy has also been roughly estimated to be $\gtrsim 1.6$ eV.[20] While the dissociation of the divacancy requires higher energy (at least equal to binding energy) than the diffusion process, dissociation can still be a competing or dominant process with diffusion in systems where there are relatively few sinks.

In this paper, we report a detailed study of the annealing kinetics of the electron-induced defects associated with the divacancy. The activation energy for the thermal anneal (under zero bias) is $U = 1.47 \pm 0.15$ eV. We also report the activation energies and production rates as a function of the energy of the bombarding electron beam. The capture cross sections for majority carriers from these levels are also reported. Deep level transient spectroscopy[23] has been used in these studies.

II. EXPERIMENTAL PROCEDURE AND RESULTS

A. Defect spectroscopy

The samples used in these studies (p^+nn^+) were fabricated from an ultrapure-floating-zone dislocation-free n-type silicon substrate that is normally used in the fabrication of high-voltage rectifiers and thyristors. The resistivity of the starting material is 25–35 Ω cm. The p^+ layer is doped to 10^{19} cm^{-3} with boron and the n^+ layer is doped to 10^{21} cm^{-3} with phosphorus. Even though the starting material is a floating-zone silicon, the fabricated devices contain oxygen. The oxygen was introduced during the p^+ and n^+ diffusions. Since the p^+ and n^+ layers are so heavily doped, the DLTS spectrum is due only to deep levels on the lightly doped n side. The samples were then irradiated with 1.5-MeV- and 3-MeV-electron beams to a flux of 2.8×10^{14} and 7×10^{14} electrons/cm^2, respectively. For the 1.5-MeV radiation, the samples were mounted on a cooling block and the temperature of the samples did not rise above room temperature during radiation. The temperature of the samples irradiated at 3 MeV was not so monitored but it is believed that the temperature rise in these samples was less than 20 °C, certainly not enough to anneal the electron-induced defects. The 3-MeV irradiations were done at the Electronized Chemicals Corporation, Burlington, Mass.

The defect spectrum was obtained by the technique of deep level transient spectroscopy (DLTS).[23,24] In the DLTS technique, a fabricated p^+nn^+ diode is reverse biased, say to 6 V, and the junction is repetitively pulsed from −6 up to 0 V electrically (introducing majority carriers into the depletion region). Electron emission from the defects in the upper half of the energy gap can be observed following each pulse in the form of capacitance transients. Levels in the lower half of the band gap can be observed by repetitively pulsing the junction to forward bias. These transients are detected by a sensitive capacitance bridge operating at 20 MHz and a boxcar integrator which has been tuned to a given emission rate. As the temperature is scanned from 77 to 300 °K, a peak is observed in the spectrum when the emission rate of a particular defect equals the selected "rate window".[23] Figure 1 shows the defect spectrum resulting from the 1.5-MeV irradiation. Three electron traps (A1 through A3) and one hole trap H1 were introduced by radiation. In terms of induced defects there is no difference between 1.5-MeV- and 3-MeV-

 Copyright © 1976 American Institute of Physics

Downloaded 13 Jun 2013 to 128.210.126.199. This article is copyrighted as indicated in the abstract. Reuse of AIP content is subject to the terms at: http://jap.aip.org/about/rights_and_permissions

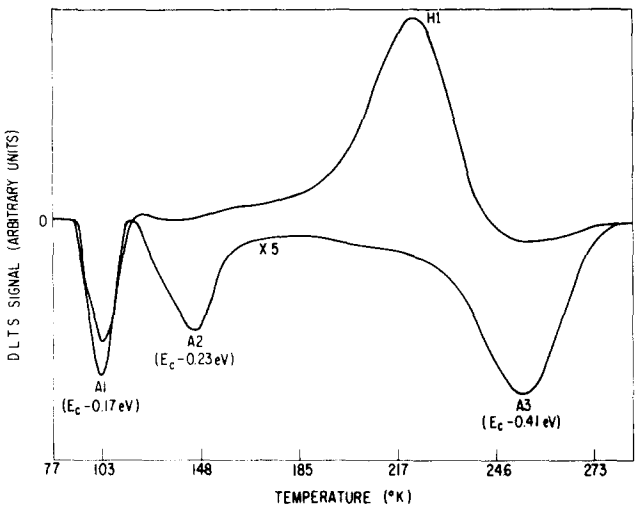

FIG. 1. DLTS spectrum of 1.5-MeV-electron irradiation-induced defects in n-type silicon. A1 through A3 are electron traps and H1 is a hole trap.

irradiated samples although the concentrations of the defects in 3-MeV-irradiated samples are higher as expected. A1 is the well-characterized A center which is the oxygen-vacancy pair. No attempt is made in these studies to further characterize it.

The electron capture cross sections at A2 and A3 were determined by the usual technique of varying the majority-carrier pulse duration.[23,24] Figure 2 shows the plot of $\ln\{[N_\infty - N(t)]/N_\infty\}$ versus pulse duration for the two levels (A2 and A3) where $N(t)$ is the concentration of the defect at a pulse width, t, and N_∞ is the saturation value of the concentration of the defect. The slopes of the straight lines through the data points give the electron capture rates at these levels. The electron capture cross sections at A2 and A3 (as determined from the capture rates) are 0.6×10^{-16} and 1.62×10^{-16} cm^2, respectively.

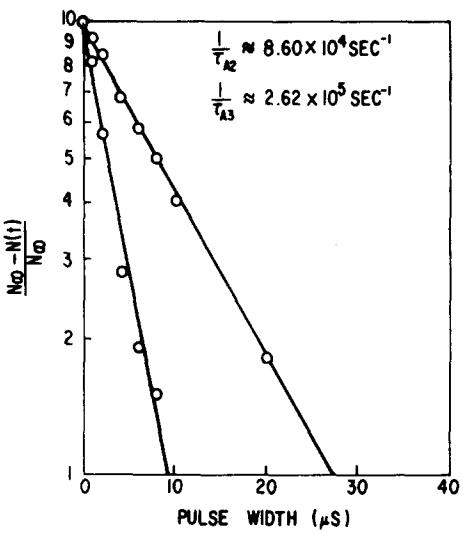

FIG. 2. The dependence of filled traps A2 and A3 on pulse duration. The slopes of the straight lines through the data points are the electron capture rates.

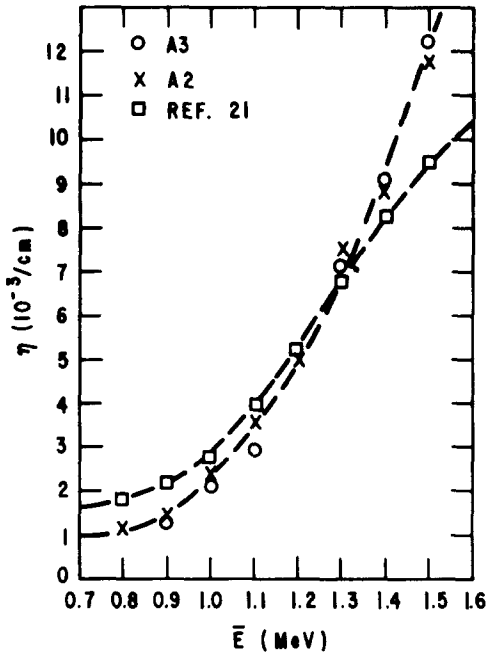

FIG. 3. Production rates of A2 and A3 versus electron energy. Also shown is the production rate of the divacancy as studied by Corbett and Watkins (Fig. 2 of Ref. 21).

The production rate studies of A2 and A3 were carried out in the energy region 0.8—1.5 MeV. The energy of the electron beam was varied in steps of 0.1 MeV while keeping the flux of 2.8×10^{14} electrons/cm^2 fixed for each sample. The introduction rate of the defects was then obtained from

$$\eta = N_{TT}/\Phi,$$

where N_{TT} is the concentration of the defect and Φ is the flux. Figure 3 shows the results of the production rate studies of both A2 and A3 in this energy range. As we can see, the introduction rates for A2 and A3 are identical. Also shown in Fig. 3 are the production rate studies of the divacancy in the energy region 0.8—1.5 MeV by Corbett and Watkins.[21] The agreement, which is quite remarkable, suggests that A2 and A3 defects are associated with the divacancy.

B. Defect annealing

The annealing of the samples was performed in an argon atmosphere in a furnace which was controlled within an accuracy of ±0.5 °C. In addition to monitoring the furnace temperature, the temperature of the sample also was monitored with a thermocouple imbedded in it. The thermal rise time of the sample to the annealing temperature is about 30 sec.

The DLTS spectrum was recorded after each annealing step at a fixed temperature. The annealings at the relatively low temperatures (250, 260, and 270 °C) were carried out for 1 h at a time. The 280 °C anneal was for 30 min, while the annealings at 290, 300, 310, and 320 °C were 20-min steps. Those at 330 and 340 °C were 10-min steps; the annealings at these higher temperatures were much faster, as expected. Figure 4 shows

Downloaded 13 Jun 2013 to 128.210.126.199. This article is copyrighted as indicated in the abstract. Reuse of AIP content is subject to the terms at: http://jap.aip.org/about/rights_and_permissions

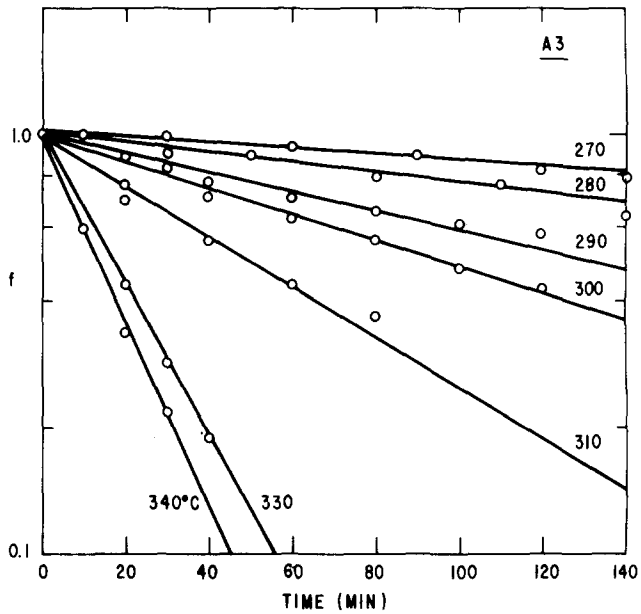

FIG. 4. DLTS signal of level A3 as a function of annealing time at various temperatures.

the fraction of the remaining defect (for the A3 level) after each annealing step. The annealing reaction is first order and follows this simple exponential expression[25]

$$f = N(t)/N_0 = \exp(-t/\tau), \tag{1}$$

where τ is the annealing rate. The slope of the straight line through the data points in Fig. 4 is the annealing rate at that particular temperature.

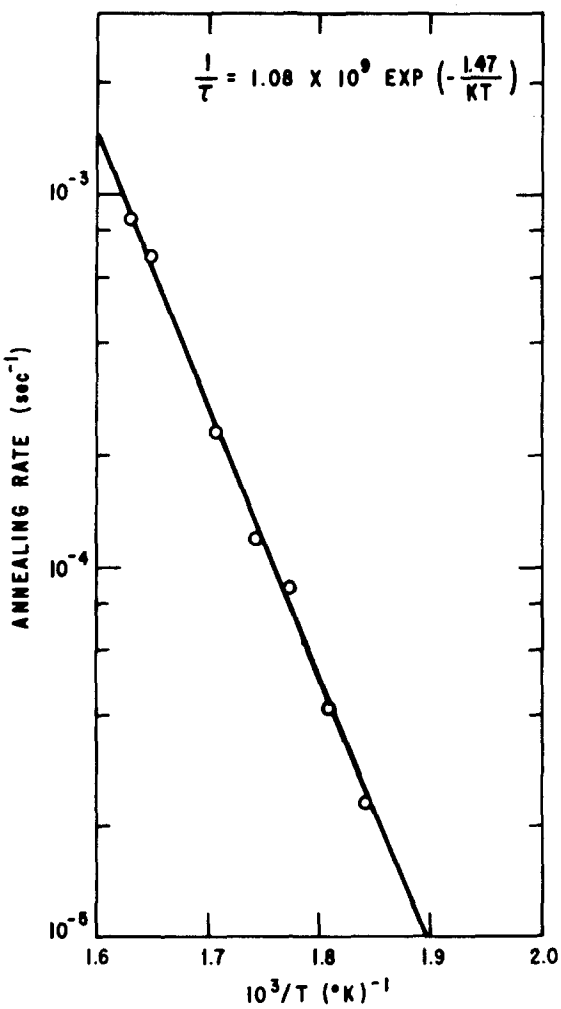

FIG. 5. Annealing rate of the A3 level, as obtained from Fig. 4, versus inverse temperature for zero bias.

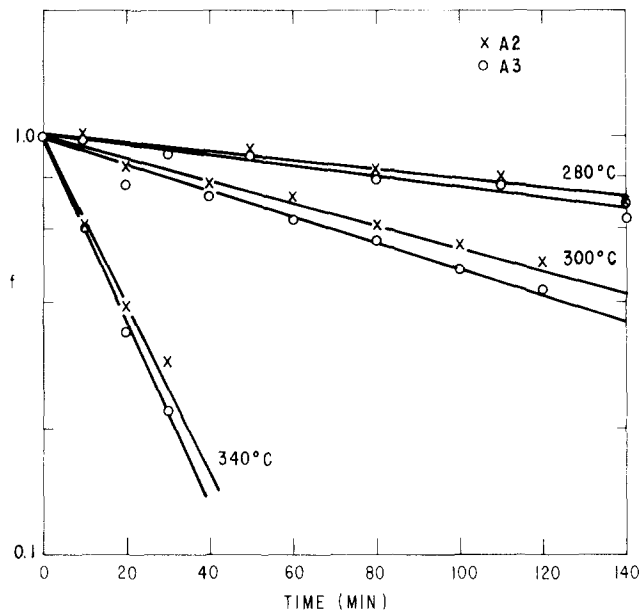

FIG. 6. DLTS signal of levels A2 and A3 as a function of annealing time at arbitrarily chosen temperatures. Note the similarity of the annealing behavior of the two defects.

For thermally activated reaction, the annealing kinetics are completely determined by

$$\frac{1}{\tau} = \frac{1}{\tau_0} \exp\left(\frac{-U}{kT}\right), \tag{2}$$

where $1/\tau_0$ is the frequency factor and U is the activation energy for the thermal anneal. Figure 5 shows the plot of annealing rate (as determined from Fig. 4) versus inverse temperatures. The slope of the straight line through the data points in Fig. 5 gives the activation energy for the thermal anneal, which is found to be 1.47 ± 0.15 eV, and a frequency factor of 1.08×10^9 sec^{-1}.

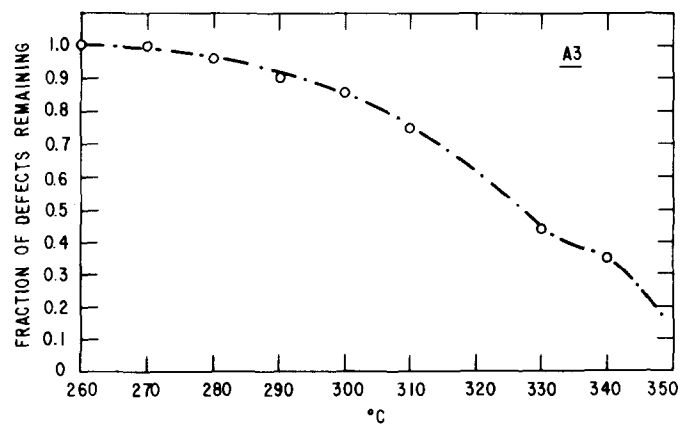

FIG. 7. Isochronal anneal (20 min at each temperature) of A3 level in floating-zone n-type silicon. The A2 level follows similar curve with $1/e$ point $\approx 340\,^{\circ}\text{C}$.

Downloaded 13 Jun 2013 to 128.210.126.199. This article is copyrighted as indicated in the abstract. Reuse of AIP content is subject to the terms at: http://jap.aip.org/about/rights_and_permissions

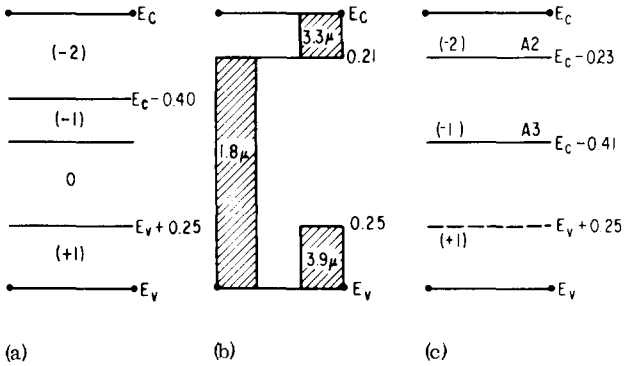

FIG. 8. (a) The energy levels in the forbidden gap corresponding to the different charge states of the divacancy deduced from EPR studies; (b) The Fermi-level dependence of the ir bands found by Fan and Ramadas. The shaded areas indicate the range in Fermi-level position over which band is observed. (c) The new charge state assignments of the levels associated with the divacancy.

Figure 6 shows the comparison between the annealing behavior of the two defects at arbitrarily chosen temperatures. As we can see, the two defects show (within experimental error) the same annealing behavior. It is interesting to point out that other defects, not produced directly by electron bombardment, appear at various stages of the annealing process. Most of these secondary defects anneal out before 350 °C. A detailed study of these secondary defects will be reported elsewhere.

Figure 7 shows the 20-min isochronal anneal of level A3. We can see that there is practically no annealing below 280 °C. The $1/e$ point is at 340 °C.

III. DISCUSSION

The divacancy is believed to introduce three energy levels in the band gap at $E_c - 0.4$ eV,[11,20] $E_c - 0.54$ eV,[11] and $E_v + 0.25$ eV,[20] so the presence of the divacancy would be detected by observing three activation energies with an identical introduction rate and the same annealing behavior. The production rate and the annealing behavior of A2 and A3 are identical; this alone suggests that A2 and A3 are different charge states of the same defect. The agreement of the production rates of A2 and A3 with the production rate of the divacancy, on the other hand, strongly suggests that A2 and A3 can be associated with the divacancy.

The 1.8-, 3.3-, and 3.9-μ bands in the ir spectrum have been associated with the divacancy.[22] According to Fan and Ramadas,[10] the appearance and disappearance of these bands in the ir spectrum depend upon the position of the Fermi level. From Fig. 8 (Fig. 4 of Ref. 22 is reproduced here as Fig. 8 for the purpose of discussions) we see that the Fermi level must be below $E_c - 0.21$ eV, above $E_c - 0.21$ eV, and below $E_v + 0.25$ eV for the appearance of 1.8-, 3.3-, and 3.9-μ bands, respectively. It has been suggested[22] that the 1.8-μ band disappears from the ir spectrum when the divacancy changes from a single-minus charge state to a double-minus charge state. This change, according to infrared absorption experiments, occurs at a level around $E_c - 0.21$ eV. However, this change to double-minus charge state has been estimated from EPR studies to occur at $E_c - 0.41$ eV. This apparent discrepancy probably results from the difficulty of monitoring the Fermi level versus emergence of the relevant EPR or ir spectrum, especially if the defect of interest is not the dominant one. The association of A2 ($E_c - 0.23$ eV) and A3 ($E_c - 0.41$ eV) with the divacancy is quite significant in the attempt to resolve this discrepancy. From the electrical energy positions of A2 and A3, we may correlate the A2 level with the double-minus charge state and the A3 level with the single-minus charge state of the divacancy. This new charge state assignment is consistent with EPR studies in regard to the number of energy levels corresponding to the different charge states of the divacancy.

The electron capture cross sections at A2 and A3 are other pieces of evidence that seem to support the charge state assignments of the divacancy. The measured capture cross sections for A2 and A3 [$(0.6 - 1.62) \times 10^{-16}$ cm^2] are quite reasonable in relation to one another. Since A2 is the double-minus charge state, it should have a smaller electron capture cross section because of its larger Coloumbic repulsive force. Actually, the electron capture rate at A3 (see Fig. 2) is about three times faster than that at A2, though one would expect a much smaller electron capture cross section ($\sim 10^{-21}$–10^{-22} cm^2) at localized single-minus or double-minus charge sites. The divacancy, however, is highly distorted[26] and the Coloumbic force may not be as important. A detailed theoretical study is needed in this area to help us understand the capture nature of the divacancy.

The single positive charge state ($\sim E_v + 0.25$) of the divacancy was not observed in these devices. The hole trap H1 does not have an identical annealing behavior or the same introduction rate as A2 and A3. Therefore, H1 cannot be associated with the divacancy. Kimerling[27] has seen a level at $E_v + 0.28$ eV that he associates with the divacancy.

Both our isothermal and isochronal studies show higher annealing temperatures than Chen *et al.*[22] reported. Their isochronal anneal (20 min at each temperature) of 1.8- and 3.3-μ bands shows some annealing around 200 °C and only 20% of the original defect remaining at 300 °C. Our isochronal anneal studies (20 min at each temperature) shown in Fig. 7 indicate that there is practically no annealing below 280 °C and that the $1/e$ point is around 340 °C. These annealing studies are, however, consistent with those reported by Watkins and Corbett.[20]

We report an activation energy for thermal anneal of 1.47 eV with a frequency factor of $\sim 1.1 \times 10^9$ sec^{-1}. If the divacancy (in the case of diffusion to sinks) makes $\sim 10^5$ jumps before anneal, the observed frequency factor would be $\sim 10^8$ sec^{-1}. On the other hand, if dissociation is the sole mode of divacancy removal from these devices, the frequency factor would be $\sim 10^{13}$ sec^{-1}. The frequency factor of 1.1×10^9 sec^{-1}, coupled with the fact that we obtain a higher activation energy than Chen *et al.*,[22] suggests that we are probably in a regime where the two processes are taking place. The appearance of secondary defects as A2 and A3 anneal out can then be

Downloaded 13 Jun 2013 to 128.210.126.199. This article is copyrighted as indicated in the abstract. Reuse of AIP content is subject to the terms at: http://jap.aip.org/about/rights_and_permissions